World Conference on
Timber Engineering
Oslo 2023

DEVELOPMENT OF THE ANALYTICAL METHOD TO REPRODUCE SEISMIC BEHAVIOR OF CLT BUILDINGS AT LARGE DEFORMATION

So Momose[1], Tatsuya Miyake[2], Hiroshi Isoda[3], Takafumi Nakagawa[4]

ABSTRACT: Understanding the seismic resistance mechanisms and safety limits of cross-laminated timber (CLT) buildings is critical. However, the knowledge of shaking table tests of CLT buildings is limited. As a first step toward collapse analysis, in this study, it was attempted to reproduce full-scale two-story shaking table test results with maximum interstory drift of 8.77%. For that, the results which matched the experimental results were searched by performing data assimilation. Consequently, the analysis results after assimilation agreed well with the experimental results, indicating the validity of this study's analytical method, but the trend of the analytical results have to be addressed in the future.

KEYWORDS: CLT building, Large deformation, Reproductive analysis, Shaking table test

1. INTRODUCTION

The seismic performance of CLT buildings has been investigated using monotonic and quasistatic cycle tests on full-scale CLT buildings [1,2]. In 2007, full-scale shaking table tests of three-, and seven-story CLT buildings were performed as part of the Construction System Fiemme (SOFIE) project [3,4]. During the tests, no residual damage was observed after the destructive earthquakes. The maximum interstory drift of the seven-story building was 67 mm, which was 2.2% against the story height of 3.1 m between the second and third floors of the building during the Japan Meteorological Agency (JMA) Kobe 100%. Further, a five-story CLT building with narrowed panel CLT was tested on a shaking table [5]. During the JMA Kobe 100% test, the compressive rupture of CLT and yielding of all tensile bolts were observed, and a maximum interstory drift of 3.7% was measured on the Y0 plane on the second story. In the USA, a full-scale shaking table test of a two-story CLT building with replaceable components has been performed in a series of research projects on CLT buildings [6]. Interstory drift 4.29% during the Northridge of MCE+ hazard level was measured. In this study, we attempted to reproduce a shaking table test with a maximum interstory drift of 8.77% via numerical analysis, which was 263 mm for a floor height of 3 m at JMA Kobe 140% intensity, exceeding the abovementioned values.

In earthquake-prone areas, such as Japan, USA, and Italy, it is critical to clarify the safety limits and collapse mechanism of CLT buildings through collapse experiments and reproductive analysis as well as to achieve accurate seismic performance evaluation of CLT buildings to protect human lives in the event of a massive earthquake. Consequently, the authors developed the analysis software "wallstat" [7], which is based on the extended distinct element method (EDEM). In this study, the authors modified and developed "wallstat" for CLT buildings. Using the developed software, we attempted to reproduce the experiment results when CLT buildings encountered large deformation. Elemental experiments were used to define the mechanical properties of CLTs and joints. According to a previous study [8], the simple combinations of elemental experiments cannot accurately reproduce full-scale experimental results. An analysis called data assimilation [9] was performed. The process of data assimilation is shown in Fig. 1. First, spring and element parameters were multiplied by the correction factors to create various skeleton curves for the spring. Then, the analytical and experimental results were compared in terms of only the shear force–interstory drift of the first story; finally, the analytical results with the smallest error from the experimental results was extracted. Consequently, the experimental results were reproduced, and the validity of the analytical method was confirmed. Afterward, the analysis results before and after the data assimilation were compared, and the causes of the differences were discussed. This paper is part of the project funded by the Japanese forest agency and includes content that has been in press [10].

2. OUTLINE OF ANALYSIS METHOD

Previous research [11-14]. has widely used numerical calculations based on FEM, as represented using the matrix method, for the time history response analysis of buildings. However, FEM is a tool developed for the stress analysis of continuum, and geometric and material nonlinearities must be considered to trace a specimen to failure analytically. In particular, the problem of handling disproportionate forces in the calculation arises for extreme failures such as member rupture (wood fracture)

[1] So Momose, RISH, Kyoto university, Japan, momose.so.72w@st.kyoto-u.ac.jp
[2] Tatsuya Miyake, Nihon System Sekkei Architects & Engineers Inc., Japan, miyake@nittem.co.jp
[3] Hiroshi Isoda, RISH, Kyoto university, Japan, hisoda@rish.kyoto-u.ac.jp
[4] Takafumi Nakagawa, RISH, Kyoto university, Japan, nakagawa@rish.kyoto-u.ac.jp

https://doi.org/10.52202/069179-0340

and crack propagation. The individual element method [15] is an analytical method that solves these problems and can trace the collapse process. The distinct element method, also known as the "discontinuity analytical method" (a method for calculating the behavior of discrete objects), was originally developed to calculate the collapse of soil and bedrock; hence, it can naturally analyse large deformations and collapse. EDEM [16] is an extended method in which the distinct element method's discontinuum elements are connected by springs, allowing the behavior of the continuum before failure to be tracked. To reproduce the behavior as continuum before failure as in FEM, "wallstat" uses beam elements. Shear, rotational, tensile–compressional, truss springs, and beam elements, which are commonly used in structural analysis in architecture, are incorporated between the elements as springs in EDEM. This has successfully reproduced the rocking and collapse behaviors of low-rise conventional-axle construction buildings [17-21]. "Wallstat" was used to analyse CLT buildings in this study by incorporating multiple-spring (described in Fig. 11) and shear spring models to account for the rocking behavior of CLT panels.

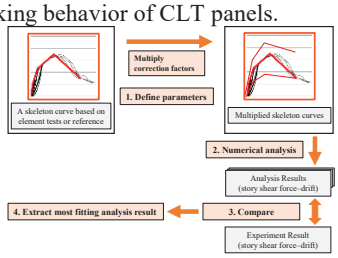

Fig. 1: *Overview of data assimilation*

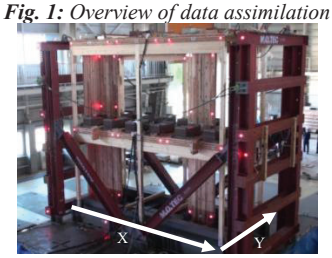

Fig. 2: *Specimen of shaking table test*

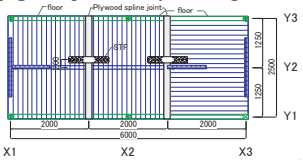

(a) Floor plan of second story

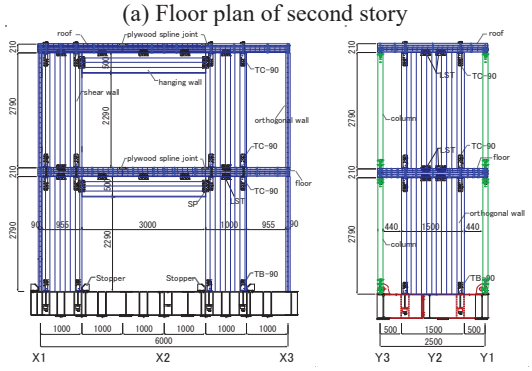

(b)Y2 plane (c)X1 plane

Fig. 3: *Floor plan and elevation of the specimen*

3. SHAKE TABLE TESTS

Fig. 2 shows the specimen of the shaking table test. The test specimen is a full-scale two-story CLT building with a narrow panel frame, consisting of a gravity frame and CLT wall, floor and roof. the floor plan of the second story (Fig. 3(a)), and its elevation in the Y2 and X1 planes where the CLT shear walls were located (Fig. 3(b, c)) are shown. The specimen size is 6.0 m long in the X direction, 2.5 m wide in the Y direction, and 6.0 m high. Two arrangements were made for the floor, one with the outermost lamina parallel to the X direction and the other with a perpendicular one, to verify various conditions. As the main seismic structure, two CLT shear walls were at the center along the X direction on the first and second stories. The strength grading of glulam, which is E95-F315, is specified in the Japan Agricultural Standard.

The meaning of E95 is the laminas in all layers have an average Young's modulus of 9.5 kN/mm^2 and above, whereas F315 means the bending strength of the glulam is 31.5MPa. The material of columns and beams was Glued Laminated Timber (Glulam) made of Scotch pine (*Pinus sylvestris*), which have 2 different strength grading of E95–F315 and E105–F300. The cross-section area was 120 (width) × 120 (height) mm, 120 (width) × 300 (height) mm, respectively. The horizontal diaphragm was made up of seven-layered 210-mm thick CLT panels of Japanese cedar (*Cryptomeria japonica*) grade Mx60 in JAS. The average Young's modulus of the lamina in the outer layers was equal to or more than 6.0 kN/mm^2, whereas it was 3.0 kN/mm^2 in the inner layers. The vertical diaphragm, e.g., shear wall, hanging wall, and orthogonal wall, comprised three-layered 90-mm thick CLT panels of Japanese cedar grade S60, meaning that the average Young's modulus of the lamina in every lamina was equal to or more than 6.0 kN/mm^2.

Fig. 4 shows details of the connectors and which spring corresponds to, and Fig. 5 shows images of the joints. Tensile bolts (ABR490, M16) and U-shaped connectors (TB-90) with holes for screws were used in the wall–foundation joints. Further, it is not common in Japan to install a stopper to resist shear force, but the purpose of this experiment was to excite up to a large deformation domain. Thus, stoppers were introduced to prevent the experiment from stopping early due to the shear failure of the CLT shear wall foot of the first story [Fig. 5(a)]. The metal protectors were attached between the wall panel and stoppers to prevent the shear wall from being embedded in the stoppers due to drifting during excitation. At the wall–wall and wall–roof joints, bolts (ABR490, M20) and U-shaped metal connectors (TC-90) with holes for screws were used as tensile connectors [Fig. 5(b)], and angle brackets (LST) with holes for screws were used as shear connectors [Fig. 5(c)]. Wall–hanging wall and floor–floor connections were made with steel plates secured with screws [Fig. 5(d)]. The screw STS6.5F was used for plywood and long steel plates in the floor–floor shear joint, and STSC65 was used for other joints. The specimen was designed according to "Route 1" provided in CLT manual [Japan Housing and Wood Technology Center Design and construction manual for CLT buildings, 2016]. "Route 1" was the simple method of allowable stress design against

https://doi.org/10.52202/069179-0340

0.2 base shear capacity for moderate earthquake and ultimate strength design against 1.0 base shear capacity for maximum considerable earthquake. The total seismic weight of the specimen was set to 175.95 kN based on the specimen specifications according to the Japanese building standard law (Notification 611 of the Ministry of Land, Infrastructure, Transport and Tourism (2016)).

As shown in Table 1, the specimen was subjected to sine wave of which the frequency was constant in Sequence 0, and the north–south (N–S) component of JMA Kobe waves, which was recorded during the Osaka–Kobe Earthquake in 1995, at 100% and 140% intensity in Sequence 1 and 2, respectively. The exciting direction was the X direction. The acceleration response spectrum of the three seismic waves is presented in Fig. 6.

The displacement where the stickers and LED lights as showed in **Fig. 5**((a)~(c)) were attached was measured with cameras, which is called "image measurement".

Fourier transformation was performed on the acceleration response time history on the shaking table and on the roof of the specimen in Sequence 0, Sequence 1, and Sequence 2; then, the Fourier spectrum was calculated. The Fourier spectrum of the roof was divided by that of the shaking table to obtain a spectral ratio (transfer function), and the lowest frequency among the peaks of the spectral ratio was defined as the natural frequency. In addition, the base shear capacity was derived from dividing the maximum shear force by the total seismic weight, in which the maximum shear force was determined from the acceleration observed during excitation. **Table 2** shows the natural frequency and base shear capacity. The specimen's maximum overall drift and interstory drift in Sequences 1 and 2 are listed in Table 3. During Sequence 1, the maximum roof displacement was 200 mm, corresponding to 3.33% overall drift. A split was seen at the edge of the CLT shear wall due to pulling by the hanging wall, but there was no significant damage other than the split [Fig. 7(a)]. During Sequence 2, the maximum roof displacement was 397 mm, corresponding to 6.62% overall drift, and the interstory drift of the first story was 8.77%. In addition, wall head embedment into the floor panel was observed [Fig. 7(b)]. No repair work was performed after Sequence 1. Some damage and deterioration in the specimen from Sequence 1 was considered in the analysis because the numerical models were subjected to Sequence 1 and 2 in a row.

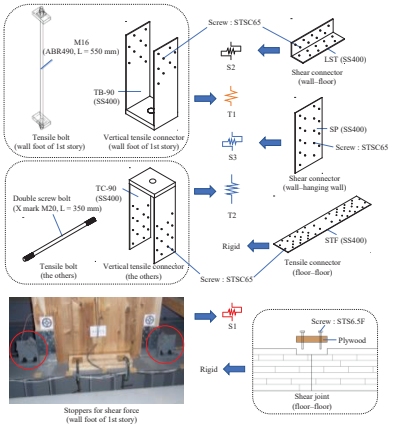

Fig. 4: *Details of connectors and the corresponding springs*

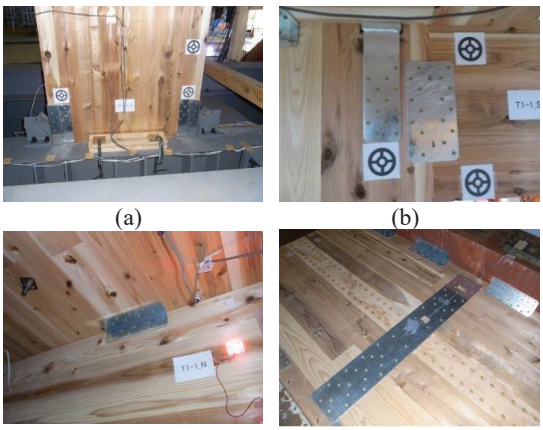

(a) (b) (c) (d)

Fig. 5: *Pictures of the joints*

Table 1: *Input seismic waves*

Sequence	Input seismic waves
0	Sine wave
1	JMA Kobe 100%
2	JMA Kobe 140%

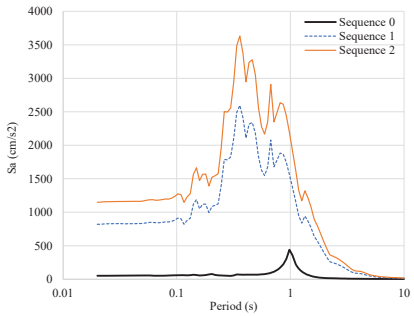

Fig. 6: *Acceleration response spectrum of input waves*

Table 2: *The natural frequency and base shear capacity in Sequence 0, 1, and 2*

Sequence	Natural frequency (Hz)	Max shear force (kN)	Total seismic weight (kN)	Base shear capacity
0	3.198	–		–
1	1.379	244.8	175.95	1.391
2	0.9155	281.0		1.597

Table 3: *Maximum overall and interstory drifts of the first story in the shaking table test*

Sequence	Max overall drift		Max interstory drift of the first story	
	(mm)	(%)	(mm)	(%)
1	200	3.33	115	3.83
2	397	6.62	263	8.77

(a) (b)

Fig. 7: *The fracture properties*

https://doi.org/10.52202/069179-0340

4. MODELING METHOD

Fig. 8 provides the analysis model created according to the joint specifications of the specimen. The number of nodes is 382 and that of springs is 668. his model was fixed in the Y direction of translation because the twisting of the specimen was not observed in the shaking table test. Fig. 9 shows the spring arrangement on the Y2 plane. The analysis model included tensile, shear, and compression springs. Two tensile springs were used for the two types of tensile joints in "wall–foundation" (T1) and "wall–wall" or "wall–roof" (T2). Three types of shear springs were inserted corresponding to the stoppers in "wall–foundation" (S1) and shear joints with steel-plated screws in "wall–floor" or "wall–roof" (S2) and "wall–hanging wall" (S3). Three differently defined compression springs were inserted to express the embedment ability of CLT under loads applied to "wall–foundation" (C1), "wall–floor, wall–roof" (C2), and "wall–hanging wall" and "orthogonal wall–floor" (C3). Other planes, such as Y1 and X1, were modeled similarly.

The modeling method for the CLT shear wall is shown in Fig. 10: the CLT shear wall was replaced by a beam element with rigid beams at its top and bottom ends corresponding to the wall width. The joints at the wall head and foot were modeled with tensile springs, shear springs, and 11 compression springs. The 11 compression springs at equal intervals was called "multiple-spring"; this modeling method has been used in some numerical analyses of specimens with CLT to reproduce the rocking behavior of the CLT shear wall [22,23]. The orthogonal walls, hanging walls, and floor panels were all modeled with beam elements and rigid beams, similar to the CLT shear walls. The beam elements were given only one Young's modulus, which was applicable for both bending and compression. The Young's modulus was set to 4.0 kN/mm^2 for CLT shear walls and hanging walls because the major direction layer was seen as 0 kN/mm^2 according to CLT manual. In addition, it was set to 2.571 kN/mm^2 for the floor panels along the major direction, and 1.285 kN/mm^2 along the minor direction. When establishing the floor panel parameters, the cooperation width was considered. The gravity frame was modeled as a beam element with elastoplastic rotational springs at the element ends. The columns and beams' Young's modulus were set to 9.5 and 10.5 kN/mm^2, respectively, and the bending strength were set to 31.5 and 30.0 Mpa, respectively. This Young's modulus was applied for both bending and compression. Nonlinear tensile shear springs were used to simulate each joint, and nonlinear compression springs were used to model the CLT's embedment properties. Fig. 11 shows hysteretic rules of tensile–compressional and shear springs. The tensile–compressional spring was modeled as a slip type in tension and elastoplastic in compression. Shear springs were set to bilinear for blind prediction, and later wall–foundation shear springs were reset to slip type considering the load–displacement relationship of the experimental results.

The ultimate capacity for tensile springs at the wall–foundation joint (T1) were determined to be 59.3 and 93 kN, and the Young's modulus and effective area of tensile bolts (ABR490, M16) were 205 kN/mm^2 and 157 mm^2 according to JIS B 1220. In addition, the length between the nuts was 400 mm, therefore, the first stiffness and the ultimate displacement for the T1 spring were set to 26.0 kN/mm and 41 mm based on CLT manual. Similarly, for the wall–wall joint (T2), the Young's modulus and effective area of tensile bolts (ABR490, M20) were 205 kN/mm^2 and 245 mm^2 according to JIS B 1220, and the length between the nuts was 200 mm. Therefore, the first stiffness and the ultimate displacement for the T2 spring were set to 30.0 kN/mm and 20 mm according to CLT manual. For shear spring at wall–floor (S2), the yielding and ultimate capacity of the two angle brackets were determined to 54 and 90 kN, respectively, based on CLT manual. In addition, considering friction, the first stiffness was assumed to be like rigid, and the value obtained by multiplying the allowable (79.6 kN) and ultimate capacity (93.0 kN) of the tensile joint from JIS B 1220 by a friction coefficient of 0.3 were added to 54 and 90 kN, which is equivalent to 77.9 and 118 kN. As the four shear springs were distributed at the wall–floor joint as Fig. 10, the calculated yielding and ultimate capacity were divided by 2. Finally, yielding and ultimate capacity for the shear spring were set to 38.9 and 59.0 kN. The ultimate displacement was set to 23.86mm based on CLT manual. Skeleton curves of the wall–hanging wall shear spring (S3) and wall–foundation compression spring (C1) were determined from the element test results (Fig. 12(c, d)). The critical tensile–compressional and shear spring properties in this analysis model are presented in Table 4 and Table 5. All analytical results were generated using a time-integration step of 10^{-6} s. The numerical analysis used the measured acceleration at the center of the shaking table as ground motions. The model weights were equal to the seismic weights of the full-scale specimen, including members and loaded weights, and the weights of the first and second stories were set to 100.54 and 75.41 kN, respectively.

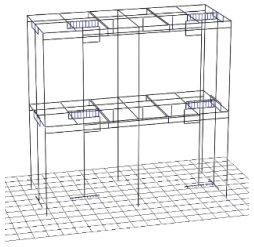

Fig. 8: *Analysis model*

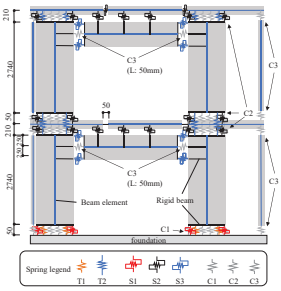

Fig. 9: *The spring arrangement on the Y2 plane*

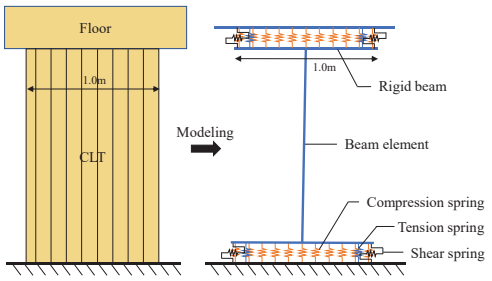

Fig. 10: *Modeling for CLT shear wall*

https://doi.org/10.52202/069179-0340

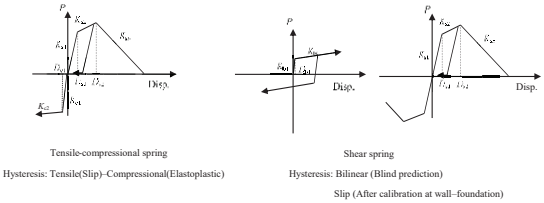

Fig. 11: *Hysteresis rules of tensile–compressional and shear springs*

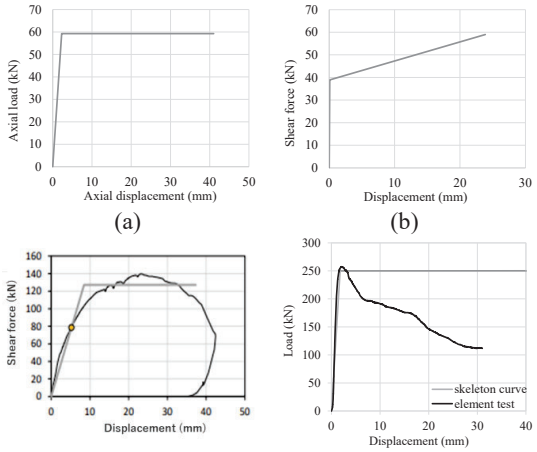

Fig. 12: *Skeleton curve of springs used in blind prediction*

Table 4(a): *Tensile–compressional spring properties based on the element tests and reference values (tensile side)*

Spring	K_{s1} (kN/mm)	K_{s2} (kN/mm)	K_{s3} (kN/mm)	D_{s1} (mm)	D_{s2} (mm)	D_{s3} (mm)
Wall–foundation (T1)	26	0.001	-0.001	2.3	40	41
Wall–wall (T2)	30	0.001	-0.001	3.1	10	20
Wall–foundation (C1)	0.001	0.0001	-0.001	13.5	21.6	1000

Table 4(b): *Tensile–compressional spring properties based on the element tests and reference values (compressional side)*

Spring	K_{c1} (kN/mm)	K_{c2} (kN/mm)	D_{c1} (mm)
Wall–foundation (T1)	0.001	–	–
Wall–wall (T2)	0.001	–	–
Wall–foundation (C1)	140.4	0.001	1.78

Table 5: *Shear spring properties based on the element tests and reference values*

Spring	K_{b1} (kN/mm)	K_{b2} (kN/mm)	D_{b1} (mm)	D_{b2} (mm)
Wall–foundation (S1)	Rigid			
Wall–floor (S2)	486.75	0.8445	0.08	23.86
Wall–hanging wall (S3)	15	0.001	8.5	37

5. BLIND PREDICTION

In the push-over analysis (blind prediction), the skeleton curves of the springs were determined based on the elemental tests results of seismic elements. The analysis results and experimental results are shown in Fig. 13. The first stiffness agreed with the experiments for both the first and second stories, but the maximum capacity of the second story and the ductility of the first and second stories were insufficient, indicating that the analysis cannot reproduce the full-scale shaking table test results when the parameters of the springs were determined by element test results as described in previous papers [8]. Thus, reproductive analysis was performed to better match the experimental results.

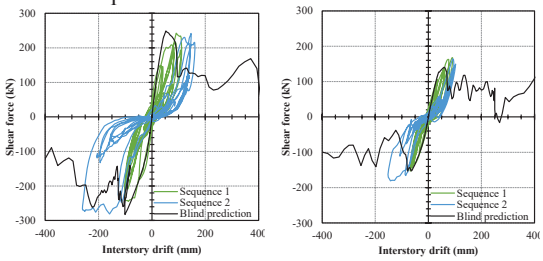

Fig. 13: *Push-over analysis (blind prediction)*

6. REPRODUCTIVE ANALYSIS METHOD

As previously stated, pushover analysis based on elemental tests and references could not reproduce the behavior of full-scale shaking table test at large deformation. The shaking table test results were used to calibrate the spring parameters for the wall–foundation tensile and shear joints (Fig. 14). For the tensile spring, the axial force–displacement relationship of the tensile bolts at the wall–foundation was traced and the skeleton curve was redefined by the slip-type hysteresis rules. In addition, a pretension load of 20 kN was added according to the experimental condition. Half of the shear force for the first story against wall–foundation relative displacement was traced for the shear spring skeleton curve. Half of that was used because there were two CLT shear walls on the first story. The skeleton curve was redefined by the slip-type hysteresis characteristics. Table 6 shows the two spring properties after calibration. Comparing the skeleton curve in blind prediction and after calibration, the tensile spring parameters after calibration matched well with those in blind prediction. For the shear spring, the difference in the first stiffness was large, indicating that the shear resistance ability of the stoppers was not rigid due to the embedment of the CLT shear wall even if the metal protectors were installed.

Further, to enhance reproducibility, the analytical method of this study [9], data assimilation, was performed for the reproductive analysis. Fig. 1 shows an overview of data assimilation executed as the reproductive analysis. The critical 24 parameters of springs and elements in **Table 7** were the target of data assimilation and multiplied by the correction factors to create various skeleton curves, and the parameter combinations when fit to the

experiment result were explored. The correction factors had the range to account for variations in materials and resistance factors which were not considered in the analytical model. Assuming the variation due to these uncertainties was expressed as the correction factors' coefficient of variation CV = 0.2 and the mean value of the correction factors μ was 1, the standard deviation σ = 0.2 was derived from Eq. (1). Assuming that the correction factor x was normally distributed, standardization was performed using the random variable z according to Eq. (2). In this case, $0.5 < x < 2.0$ accounts for 99.38% of the total, which can cover almost all patterns. Therefore, the correction factors were varied in the range of 0.5 to 2.0 with the interval of 0.15 for the Young's modulus, first stiffness, and first yield point. For the second stiffness, the correction factors were varied in the range of 0.0001 to 0.8 with the interval of 0.08, considering that the most possible values of the stiffness after yielding were covered.

$$CV = \frac{\sigma}{\mu} \quad (1)$$

$$\boldsymbol{z = \frac{x - \mu}{\sigma}} \quad (2)$$

With this method, various skeleton curves for the springs were created. Then, the experimental results and many analytical results were compared in terms of only the shear force–interstory drift of the first story through Sequence 1 and 2, not in terms of the time history of interstory drift and uplift displacement. Then, the analytical results with the smallest error from the experimental results was extracted. Later, when comparing the skeleton curves between before assimilation and after assimilation, five analysis results with the smallest five errors from the experimental results were extracted. Thus, assimilation was performed to match both Sequence 1 and 2. Therefore, the damage from Sequence 1 was also considered in the analytical results after data assimilation. In addition, because all springs and elements were free in all directions except the Y direction of translation, if multiple factors are included in the springs and elements, data assimilation of the parameters will result in an accurate analysis model.

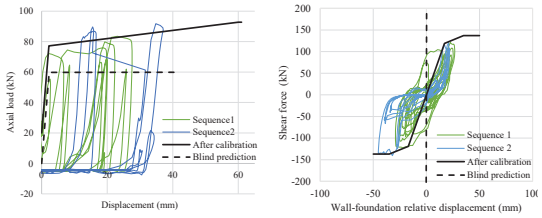

(a) (b)

Fig. 14: *The hysteresis of shaking table test and the spring skeleton curves in blind prediction and after calibration*

Table 6: *Calibrated spring properties based on the shaking table test results*

Spring	K_{s1} kN/mm	K_{s2} kN/mm	K_{s3} kN/mm	D_{s1} mm	D_{s2} mm	D_{s3} mm	K_c kN/mm
Wall–foundation (T1)	26	0.2685	-0.001	2.2	60	61	0.001
Wall–foundation (S1)	7	1	-0.001	17	35	50	–

Table 7: *The list of parameters multiplied by correction factors*

Spring position	Joint type	Spring type	Multiplied parameters
CLT shear wall	–	Beam element	Bending Young's modulus
Hanging wall	–	Beam element	Bending Young's modulus
Floor panel, beam	–	Beam element	Bending Young's modulus
Wall–wall	Tensile	Tensile–compressional	K_{s1}, K_{s2}, D_{s1}
Wall–hanging wall	Tensile	Tensile–compressional	K_{s1}, K_{s2}, D_{s1}
Column foot	Tensile	Tensile–compressional	K_{s1}, K_{s2}, D_{s1}
Wall–wall	Shear	Shear	K_{b1}, K_{b2}, D_{b1}
Wall–hanging wall	Shear	Shear	K_{b1}, K_{b2}, D_{b1}
Wall–foundation	Compression	Tensile–compressional	K_{c1}, K_{c2}, D_{c1}
Wall–hanging wall	Compression	Tensile–compressional	K_{c1}, K_{c2}, D_{c1}

7. REPRODUCTIVE ANALYSIS RESULT

The interstory drift time history for the first and second stories in Sequence 1 and 2 from data assimilation is illustrated in Fig. 15, together with the blind prediction and experimental results. The blind prediction did not agree with the experiment results except for the initial drift response to the excitation. Meanwhile, after assimilation, both the interstory drift and phase agreed well with the experimental results through Sequence 1. Even in Sequence 2, there was a slight error in interstory drift with the experiment results after the maximum drift, but the trends of the interstory drift and phase agreed well, implying a good reproduction result. Fig. 16 illustrates the shear force–interstory drift relationships for the first story in Sequence 1 and 2 in the experiment, in blind prediction, and after assimilation. For the blind prediction, the maximum load was nearly reproduced in Sequence 1, but not in Sequence 2. Nevertheless, the interstory drift and stiffness were not consistent with the experiment results. However, the analytical results after assimilation were almost identical to the experimental result, indicating that the overall behavior of the specimen could be tracked by reproductive analysis. Fig. 17 shows the uplift displacement time history at the CLT shear wall foot of the first story in Sequence 2 in the experiment and the analysis results after assimilation. The analytical result after assimilation agreed with the experimental results in drift and phase, demonstrating that the detailed behavior of the two-story CLT building was reproduced. Fig. 18 and Fig. 19 show the comparison of specimen's behavior in Sequence 1 and 2 between the experiment (red line and spheres depicted by image measurement data) and reproductive analysis (shown as Fig. 8) and the interstory drift time history (Fig. 15(a, c)) with the moment which the image exhibits. It could be seen that the analysis results agreed with the experiment results in appearance in Sequence 1 and 2. Therefore, it was verified that the analysis results were identical to the experiment results.

https://doi.org/10.52202/069179-0340

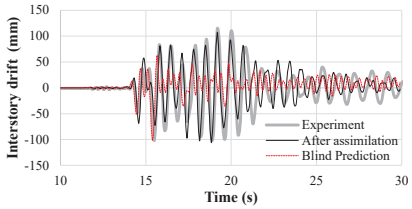

(a)First story in Sequence 1

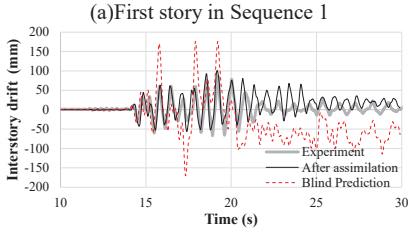

(b) Second story in Sequence 1

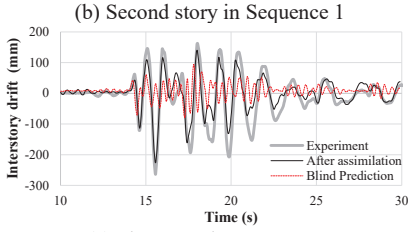

(c) First story in Sequence 2

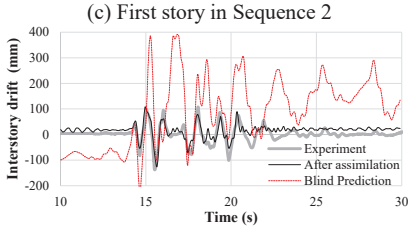

(d) Second story in Sequence 2

Fig. 15: *The interstory drift time history of the shaking table tests, blind prediction, and after data assimilation*

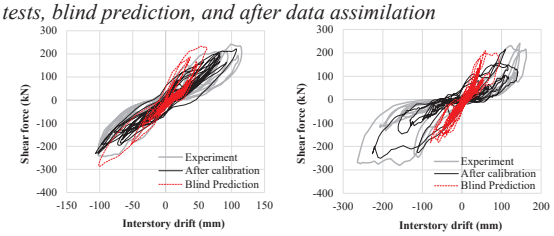

(a) Sequence 1 (b)Sequence 2

Fig. 16: *The story shear force–interstory drift relationship of the experiment, blind prediction, and after data assimilation for 1st story*

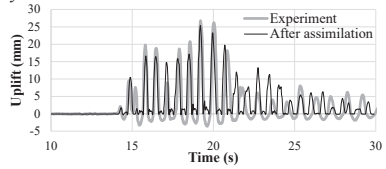

(a)Sequence 1

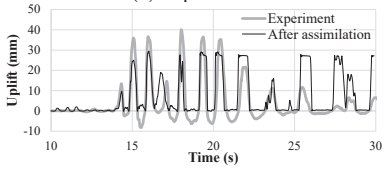

(b)Sequence 2

Fig. 17: *The time history of uplift displacement at the CLT shear wall foot for the first story in the experiment and after data assimilation*

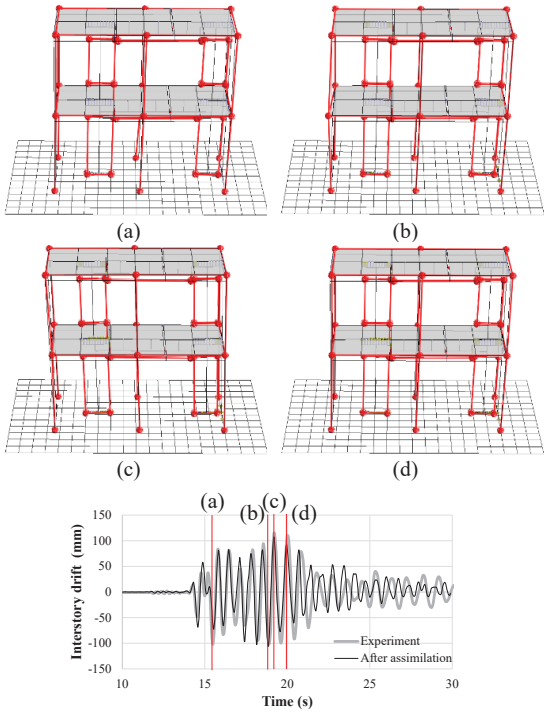

Fig. 18: *The comparison of specimen's behavior between the experiment and analysis in Sequence 1*

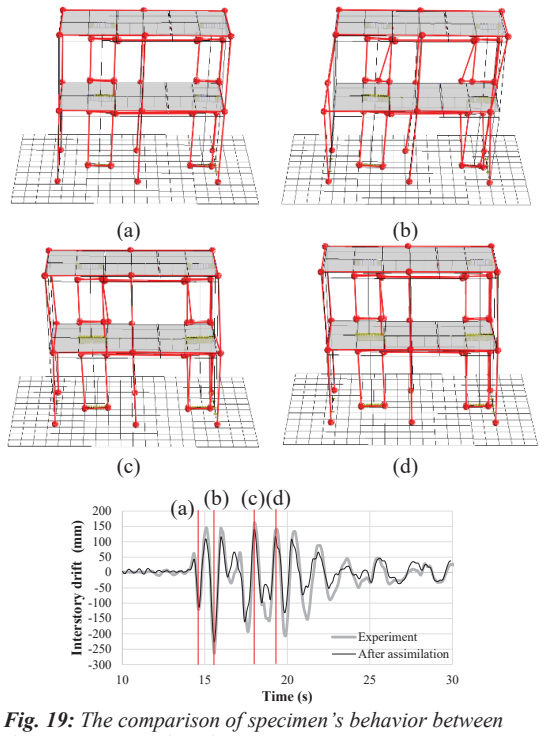

Fig. 19: *The comparison of specimen's behavior between the experiment and analysis in Sequence 2*

Fig. 20 shows the skeleton curves for the four springs before and after assimilation. The blue solid lines in each of **Fig. 20** (a)–(d) are skeleton curves in the analysis results with the five smallest errors from the experimental results. The five analytical results (smallest one was labelled (1), second smallest (2), third smallest (3), fourth smallest (4), and fifth smallest (5)) are shown to grasp the trend of how the skeleton curves changed.

For the wall–wall tensile springs (**Fig. 20**(a)), a clear trend of the first stiffness and yielding capacity was not seen. For the wall–floor shear spring (**Fig. 20**(b)) considering friction when determining the parameters, the skeleton curves tend to be the same before and after assimilation. For the wall–hanging wall shear spring (**Fig. 20**(c)) without considering friction, both stiffness and yield capacity tended to increase after assimilation. This implies that the friction between the shear connectors under suppressed force contributed to an increase in both stiffness and yielding capacity. However, it is recommended to reconsider the friction coefficient which is assumed as 0.3 in the paper. In addition, the difference in the loading speed between the dynamic loading during the full-scale shaking table test and the static loading in the element tests can be another reason because steel strength increases as the strain velocity increases. Also, for the (5), the yielding capacity of wall–floor shear spring was highest although the first stiffness and yielding capacity of wall–hanging wall shear spring were smallest, inferring that the wall–floor and wall–hanging wall shear springs were in a inverse relationship. An increasing trend of the first stiffness and yielding capacity was also seen in the case of compression springs (**Fig. 20**(d)). Similar to shear springs, the dynamic effects of loading can be a contributing factor to the increase in stiffness and yielding capacity. Another possible factor is that the dead weights were fixed to the floor with screws in the experiment, which increased the floor rigidity significantly and suppressed the vertical deformation caused by the rocking of the CLT shear walls." These inverse interaction and factors for increase of stiffness and capacity such as friction, dynamic effects, and increase of floor rigidity will be verified by comparing the detailed behavior and performing static loading tests in the future.

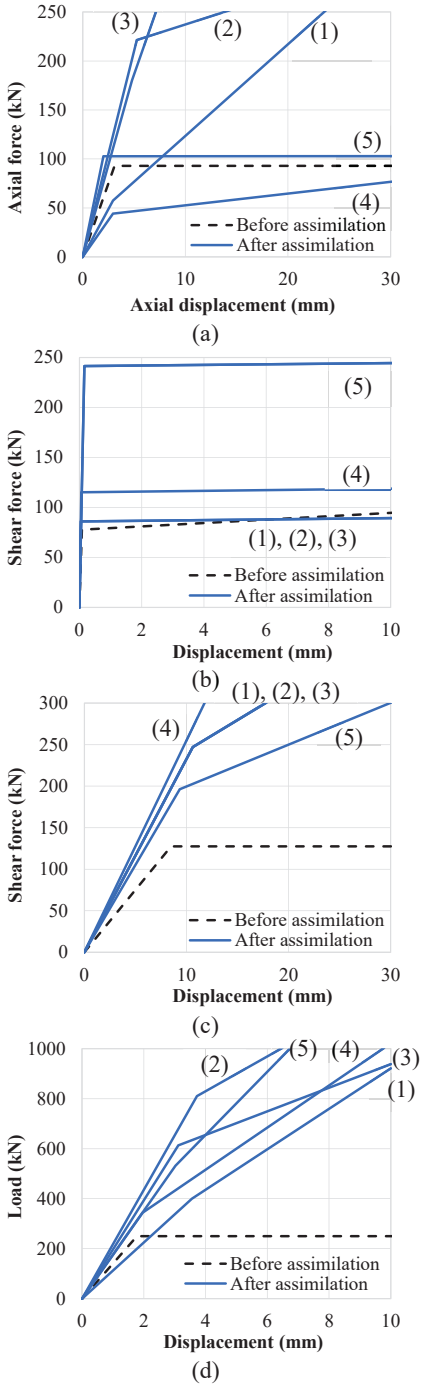

Fig. 20: *Skeleton curves of springs before and after data assimilation*

https://doi.org/10.52202/069179-0340

8. CONCLUSION

In this study, a model that can replicate the seismic behavior of CLT buildings up to a large deformation region is proposed using "wallstat," which was modified to consider the restoring force and P–δ effects due to the rocking behavior of CLT panels. The shaking table test on a two-story full-scale CLT building validated the analytical method.

- A split was observed at a wall–hanging wall joint. Despite the 8.77% interstory drift of the first story in Sequence 2, further damage, such as wall head embedment into the floor panel, was negligible.
- In pushover analysis, blind prediction agreed well with the experimental result in terms of the first stiffness but not the maximum capacity of the second story and the ductility of the first and second stories.
- The shaking table test results of the two-story full-scale CLT building were analyzed using "wallstat," which was modified to include multiple-spring and shear spring models, to account for restoring force and P–δ effects due to the rocking behavior of the CLT panels. Using wallstat, we attempted to replicate the seismic behavior of the two-story full-scale CLT building up to a large deformation domain. Blind prediction could not reproduce the experimental results in the time history interstory drift and hysteresis curves of the shear force–interstory drift of the first story. However, the analytical results after assimilation were consistent with the experimental results in interstory drift and phase in both the first and second stories although the discrepancy between the analysis and experiment after the maximum drift will be the subject of future research, demonstrating that the overall behavior of the CLT building specimen was reproduced with this analytical method even in the large deformation domain.
- The uplift displacement and phase trends of the CLT shear wall of the first story were analyzed for the uplift displacement time history. The outcomes suggest that our analysis model can even replicate the detailed behavior of a full-scale specimen at large deformation as well as the overall behavior.
- The overall behavior of analysis model could be seen identical to that of the specimen in appearance as well as on the graph.
- The skeleton curves of shear and compression springs after data assimilation tended to increase in both stiffness and yielding load compared with those before assimilation. For this, the suppression of deformation due to friction resistance, the difference in the loading speed between the element tests and the shaking table test, and the increment in floor rigidity due to fixed dead weights were considered to be the cause.

Hence, the analysis results after assimilation agreed well with the experimental results, indicating the validity of this study's analytical method. However, it is not possible to predict the responses of CLT buildings without experimental results from this study alone. In this study, as a result of varying the characteristic values for joints and members over the statistically determined range, analytical results that agree with the experimental results were obtained, and the trend of the analytical results was shown. Friction, dynamic effects, and an increase in floor rigidity due to fixed dead weights were thought to be the causes of the increase trend of stiffness and yielding capacity of shear and compression spring. In addition, as the inverse relationship between the properties of the shear springs was confirmed, the interaction among the tensile, shear, compression springs, and beam elements can also exist. These interactions in analysis models of this study have to be verified in the future through behavior comparisons of detailed part and static loading tests, and it is believed that the verification will lead to predict the seismic behavior of CLT buildings at large deformation without experimental results.

ACKNOWLEDGEMENT

This research was conducted as part of a Forestry Agency–subsidized project to study the relaxation of earthquake resistance standards by simplifying joints and reducing the number of walls, etc., based on an understanding of the seismic boundary performance of CLT panel construction method buildings. We would like to express our gratitude to all the parties involved. We used the Japan Aerospace Exploration Agency supercomputer system "JSS3" in the reproductive analysis. [24].

REFERENCES

[1] Zhang X., Isoda H., Sumida K., Araki Y., Nakashima S., Nakagawa T., Akaiyama N. 2021. "Seismic Performance of Three-Story Cross-Laminated Timber Structures in Japan" *J. Struct. Eng.*, 147 (2): 04020319. DOI: 10.1061/(ASCE)ST.1943-541X.0002897.

[2] Popovski, M., and I. Garvic. 2016. "Performance of two－storey CLT house subjected to lateral loads." *J. Struct. Eng.*, 142 (4), 2016.

[3] Ceccotti, A. 2008. "Few technologies for construction of medium－rise buildings in seismic regions." *Struct. Eng. Int.,* 18 (2), 156–165: https://doi.org/10.2749/101686608784218680.

[4] Ceccotti, A., C. Sandhaas, M. Okabe, M. Yasumura, C. Minowa, N. Kawai. 2013. "SOFIE 3D shaking table test on a seven－storey full－scale cross－laminated timber building." *Earthquake Eng. Struct. Dynam*., 42 (13), 2003–2021.

[5] Sato, M., H. Isoda, Y. Araki, T. Nakagawa, N. Kawai, and T. Miyake. 2019. "A seismic behavior and numerical model of narrow paneled cross－laminated timber building." *Eng. Struct.*, 179 (15), 9–22.

[6] Blomgren, H. E., S. Pei, Z. Jin, J. Powers, J. Dolam, J. W. van de Lindt, A. R. Barbosa, and D. Huang. 2019. "Full－scale shake table testing of cross－laminated timber rocking shear walls with replaceable components" *J. Struct. Eng.*, 145 (10): 04019115. https://doi.org/10.1061/(ASCE)ST.1943

－541X.0002388.
[7] wallstat ver.4.3.11 [Computer Software]. Research Institute for Sustainable Humanosphere, Kyoto University, Kyoto, Japan.
[8] Yasumura, M., K. Kobayashi, M. Okabe, T. Miyake, and K. Matsumoto. 2016. “Full－scale tests and numerical analysis of low－rise CLT structures under lateral loading.” *J. Struct. Eng.*, 142 (4), E4015007(12). https://doi.org/10.1061/(ASCE)ST.1943－541X.0001348.
[9] Namba, T., T. Nakagawa, Y. Kado, H. Isoda, Y. Kado, R. Odani, A. Takino. 2023. “Seismic Response Comparison of Full-Scale Moment Resisting Timber Frame and Joint Test Result” *J. Struct. Eng.* [10.1061/JSENDH/STENG-12165]. (in press)
[10] Momose S., T. Nakagawa, T. Namba, H. Isoda, and T. Miyake. 2023. “An Analytical Method to Reproduce Seismic Behavior of Two-Story Cross-Laminated Timber Building at Large Deformation” *J. Struct. Eng*. [10.1061/JSENDH/STENG-11711] (in press)
[11] Ceccotti, A., and M. Follesa. 2006. “Seismic behavior of multi－story Xlam buildings.” In *Proc., of international workshop on earthquake engineering on timber structures*., 11 University of Coimbra, Coimbra: Portugal.
[12] Dujic B., K. Strus, R. Zarnic, and A. Ceccotti. 2010. “Prediction of dynamic response of a 7－ storey massive Xlam building tested on a shaking table” In: Proceedings of WCTE 2010, world conference on timber engineering. DVD.
[13] Rinaldin, G., and M. Fragiacomo. 2016. “Non－linear simulation of shaking–table tests on 3 – and 7 – storey X－Lam timber buildings.” *Eng. Struct.*, 113 (15), 133–148.
[14] Pei, S., M. Popovski, and J. W. van de Lindt. 2013. “Analytical study on seismic force modification factors for cross－laminated timber buildings.” *Can J. Civ. Eng.*, 40 (9), 887–896.
[15] Cundall, P. A1971. “A computer model for simulating progressive, large－scale, movements, in blocky rock system.” Symposium ISRM, Nancy, 129–136.
[16] Meguro, K., and M. Hakuno. 1991. “Simulation of Structural Collapse due to Earthquakes Using Extended Distinct Element Method.” Summaries of Technical Papers of Annual Meeting. Architectural Press Institute of Japan, 763–764.
[17] Nakagawa, T., and M. Ohta. 2003. “Collapsing process simulations of timber structures under dynamic loading I: simulations of two－story frame models.” *J. Wood Sci.,* 49 (5), 392–397.
[18] Nakagawa, T., and M. Ohta. 2003. “Collapsing process simulations of timber structures under dynamic loading II: simplification and qualification of the calculating method.” *J. Wood Sci.*, 49 (6), 499–504.
[19] Nakagawa, T., T. Hidaka, and M. Inayama. 2013. “Damage investigation and collapsing process analysis of Myokenji Hondo damaged from the Great East Japan EARTHQUAKE: Part 2 Collapsing process analysis using 3D space frame model.” [In Japanese.] *J. Struct. Eng. B AIJ*, 59B, 573–578.
[20] Hidaka, T., T. Nakagawa, and M. Inayama. 2013. “Damage investigation and collapsing process analysis of Myokenji Hondo damaged from the Great East Japan EARTHQUAKE: Part 1 Damage investigation and measurement survey.” [In Japanese.] *J. Struct. Eng. B AIJ*, 59B, 567–572.
[21] Sumida, K., T. Nakagawa, and H. Isoda. 2020. “Seismic testing and analysis of rocking motions of Japanese after and－beam construction.” *J. Struct. Eng.*, 147 (2), 04020323.
[22] Sato, M., H. Isoda, Y. Araki, T. Nakagawa, T. Miyake. 2017. “Proposal of analysis model of CLT structure for small width panel and accuracy verification intended.” [in Japanese.] *J. Struct. Constr. Eng*., 82 (741), 1719–1726.
[23] Azumi Y., T. Miyake, K. Matsumoto, I. Sakurai, and N. Kawai. 2019. “A study on expansion and improvement of the structural design method for CLT panel construction, Part 2 Simplification of numerical analysis model by Multiple Spring element.” *Summaries of Technical Papers of Annual Meeting,* Architectural Institute of Japan, [In Japanese.] 461–462.
[24] JSS3 [Supercomputer]. Japan Aerospace Exploration Agency, Ibaraki, Japan

https://doi.org/10.52202/069179-0340